Journal of Power Sources 195 (2010) 6342–6348

Contents lists available at ScienceDirect

Journal of Power Sources

journal homepage: www.elsevier.com/locate/jpowsour

Transport phenomena within the porous cathode for a proton exchange membrane fuel cell

Juanfang Liu*, Nobuyuki Oshima, Eru Kurihara, Litan Kumar Saha

Graduate School of Engineering, Hokkaido University, Sapporo 060-8628, Japan

ARTICLE INFO

Article history:
Received 4 August 2009
Received in revised form 2 April 2010
Accepted 3 April 2010
Available online 18 April 2010

Keywords:
Capillary pressure continuity
PEM fuel cell
Saturation jump

ABSTRACT

A two-phase, one-dimensional steady model is developed to analyze the coupled phenomena of cathode flooding and mass-transport limiting for the porous cathode electrode of a proton exchange membrane fuel cell. In the model, the catalyst layer is treated not as an interface between the membrane and gas diffusion layer, but as a separate computational domain with finite thickness and pseudo-homogenous structure. Furthermore, the liquid water transport across the porous electrode is driven by the capillary force based on Darcy's law. And the gas transport is driven by the concentration gradient based on Fick's law. Additionally, through Tafel kinetics, the transport processes of gas and liquid water are coupled. From the numerical results, it is found that although the catalyst layer is thin, it is very crucial to better understand and more correctly predict the concurrent phenomena inside the electrode, particularly, the flooding phenomena. More importantly, the saturation jump at the interface of the gas diffusion layer and catalyst layers is captured, when the continuity of the capillary pressure is imposed on the interface. Elsewise, the results show further that the flooding phenomenon in the CL is much more serious than that in the GDL, which has a significant influence on the mass transport of the reactants. Moreover, the saturation level inside the cathode is determined, to a great extent, by the surface overpotential, the absolute permeability of the porous electrode, and the boundary value of saturation at the gas diffusion layer-gas channel interface. In order to prevent effectively flooding, it should remove firstly the liquid water accumulating inside the CL and keep the boundary value of liquid saturation as low as possible.

1. Introduction

In most of previous polymer electrolyte membrane fuel cell (PEMFC) numerical simulations [1–3], for simplicity, the catalyst layer (CL) is considered as an interface between the proton exchange membrane (PEM) and the gas diffusion layer (GDL), and neglected its thickness and structure. However, to our knowledge, the catalyst layer is the sole component where the electrochemical reaction takes place for the entire PEM fuel cell. For a better understanding of the coupled phenomena occurring in the fuel cell, it is very necessary to treat the CL as a separate domain with finite thickness and structure [4]. On this account, various mathematical and structural models have been developed for the CL [3–8].

Up to now, the structural models of the catalyst layer in the literatures can be categorized into three classes: interface models [3], pseudo-homogenous models [6,7] and heterogeneous models [8]. In the first model, cited as Refs. [1–3], the catalyst layer is assumed to be infinitely thin, and its composition and structure are ignored by assuming that all properties are uniform throughout this layer, so that it would be regarded as an interface between PEM and GDL. The second model is an improvement one over the first one. In this model, the catalyst layer is described as a macro-pseudo-homogenous film with a porous random structure, in which solid conductive material, catalyst, electrolyte and void space are uniformly distributed. However, in the third model, the catalyst layer is assumed to consist of cylindrical or spherical pellets and the void space for gas transport. Of course, the more rigorous heterogeneous models are required to be developed to take into account the morphological properties of the CL. In this paper, the pseudo-homogenous model is adopted, because it is relatively easy to formulate and solve.

During the operation of a cell, when the generation rate of liquid water at the cathode side does not equal to its removal rate, without control, the imbalance between the generation and removal rate leads to either the membrane dehydration or/and the cathode flooding, which are both detrimental to the cell performance. In addition, because the cathode electrode is the most influential layers of the performance-controlling components in the PEM fuel cells, in the present work, the interacted phenomena of the mass-transport limitation and the flooding are mainly studied and analyzed only for the cathode electrode by the numerical simulation method.

* Corresponding author. Tel.: +81 11 706 6722.
E-mail address: vacoljf@yahoo.com.cn (J. Liu).

0378-7753/$ – see front matter © 2010 Elsevier B.V. All rights reserved.
doi:10.1016/j.jpowsour.2010.04.038

Nomenclature

a_v	specific area of the active surface, $cm^2\ cm^{-3}$
c_{O_2}	oxygen molar concentration, $mol\ cm^{-3}$
c_0	oxygen molar concentration at the inlet of GDL, $mol\ cm^{-3}$
D_{O_2}	bulk diffusivity at a gas state, $cm^{-2}\ s^{-1}$
D_{eff}	effective diffusivity of oxygen, $cm^{-2}s^{-1}$
F	Faraday constant, 96487.0 C mol^{-1}
I	exchange current density, $A\ cm^{-2}$
j_c	local transfer current density, $A\ cm^{-3}$
J	Leverett function
K	absolute permeability of a porous medium, m^2
K_{rl}	relative permeability of liquid phase, m^2
L^{CL}	thickness of the catalyst layer, μm
L^{GDL}	thickness of the gas diffusion layer, μm
M_{H_2O}	molecular weight of water, $g\ mol^{-1}$
p	operating pressure of the cell, atm
p_c	capillary pressure, atm
p_g	pressure of the gas phase, atm
p_l	pressure of the liquid phase, atm
R	universal gas constant 8.314 J $(mol\ K)^{-1}$
s	saturation of liquid water
T	operating temperature of the cell, K
μ_l	velocity of the liquid phase, $cm^{-2}\ s^{-1}$

Greek symbols

α	net transfer coefficient of water
$a_{c,c}$	charge transfer coefficient in the oxygen reduction
ε^{CL}	porosity of the catalyst layer
ε^{GDL}	porosity of the gas diffusion layer
η_c	cathode overpotential, V
θ_c	contact angle, θ
ν_l	kinematic viscosity of liquid water, $m^2\ s^{-1}$
ρ_l	density of the liquid phase, $g\ cm^{-3}$
σ	surface tension, $N\ m^{-1}$
τ^{CL}	tortuosity of the catalyst layer
τ^{GDL}	tortuosity of the gas diffusion layer

Subscripts

c	capillary/contact/cathode
g	gas phase
l	liquid phase
rl	relative value
w	liquid water
o	initial value

Superscripts

CL	catalyst layer
eff	effective value
GDL	gas diffusion layer
ref	reference value

In the paper, based on Darcy' law and Fick's diffusion law, the corresponding equations of gas and liquid water transport are developed. In addition, when the CL is treated as a separate computational domain, the interfacial condition between the GDL and the CL needs to be prescribed. In the numerous literatures, the saturation continuity is automatically satisfied, but in the present work, the capillary pressures continuity is imposed on the interface. Under this interfacial condition, the local saturation distribution in the GDL and CL and the effect factors on the liquid saturation are emphatically investigated.

2. Numerical models

2.1. Model assumptions

A schematic diagram of the modeling domain is depicted in Fig. 1. The model includes both the gas diffusion layer and catalyst layer at the cathode side of PEMFCs. Transport of oxygen gas and liquid water in the through-plane direction is taken into account.

The following assumptions are made during implementing the present simulation: (1) The gas phase obeys the ideal gas law; (2) The cell operates under the conditions of isothermal, isobaric and steady state; (3) Water produced in the electrochemical reaction is assumed only in the liquid state, which may occur when the liquid water pressure is always lower than its saturated pressure at the same temperature; (4) In the catalyst layer, liquid water in the ionomer phase is in equilibrium with one in the void space.

2.2. Transport equations

2.2.1. Transport equations for oxygen

In the porous electrode along the through-plane direction, the diffusive process is dominant for the gas transport [9]. Additionally, in the present work, the dry pure oxygen is fed as the oxidant at the cathode, so Fick's diffusion law can be used to describe the gas transport. The corresponding governing equations of oxygen gas in the GDL and CL are expressed as:

$$\nabla(-D_{eff}\nabla c_{O_2}) = \begin{cases} 0 & \text{GDL} \\ -\dfrac{j_c}{4F} & \text{CL} \end{cases} \quad (1)$$

where j_c is the local transfer current density resulted from the consumption or production of charge along the catalyst layer with the unit of $A\ cm^{-3}$ and calculated by the following Eq. (10), c_{O_2} and D_{eff} are the molar concentration and effective diffusivity of oxygen, respectively, and F is Faraday's constant.

Since both GDL and CL are the porous materials, the effective diffusion coefficients need to be utilized to take into account the effects of porosity ε and tortuosity τ of the porous medium on the fluid transport, and can be obtained by modifying the corresponding bulk diffusivity by Bruggeman correlation [10]:

$$D_{eff} = [(1-s)]^{\tau} D_{O_2} \quad (2)$$

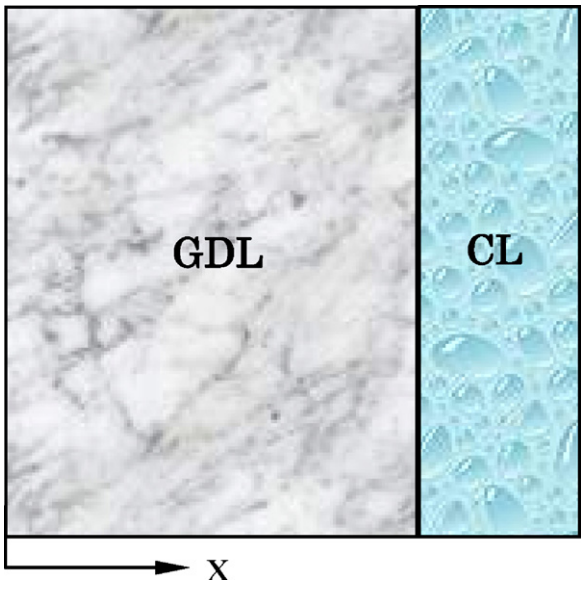

Fig. 1. Schematic picture of the computational domain.

here D_{O_2} is the bulk diffusivity of oxygen in the gas state, s is the liquid water saturation defined by the ratio between the liquid water volume and the total void volume of a porous medium. Liquid water in the electrode reduces the actual gas porosity, thereby hindering the gas transport, so the factor $(1-s)$ is employed to correct the intrinsic porosity of the porous medium.

2.2.2. Transport equations for liquid water

In the steady state, according to the conservation law and the above assumption (3), the transport equations for liquid water across the GDL and CL are given as following, respectively:

$$\nabla(\rho_l \vec{u}_l) = \begin{cases} 0 & \text{GDL} \\ \dfrac{j_c}{2F} M_{H_2O} & \text{CL} \end{cases} \tag{3}$$

where ρ_l and $\vec{u}_l$ are density and velocity of liquid water, respectively.

For liquid water in the porous electrodes, the momentum conservation also follows Darcy's law. Moreover, the dimensional scales in PEMFC geometry are very small, the gravitational effect, therefore, can be neglected. Darcy's momentum equation can be further simplified to:

$$\rho_l \vec{u}_l = -\frac{\vec{K}_{rl}}{\nu_l} \nabla p_l \tag{4}$$

in which, ν_l is the kinetics viscosity of liquid water, and $\vec{K}_{rl}$ is the relative permeability of the porous medium, which is considered the reduction in pore space available for one phase due to the existence of the other phase. Different mathematical relations between the relative permeability and the absolute one can be obtained. In the present work, the following cubic correlation [11] is used:

$$K_{rl} = s^3 K_p \tag{5}$$

where K_p is the absolute permeability of the porous electrode.

Furthermore, the liquid water pressure, denoted by p_l, can be deduced from the gas-phase pressure p_g and the capillary pressure p_c, according to [12]:

$$\nabla p_l = \nabla p_g - \nabla p_c \tag{6}$$

The gas pressure in the porous electrode changes very small along the through-plane direction [1,2], so ∇p_g can be considered as zero.

For the purpose of investigating the flooding phenomena, the transport equation of liquid water needs to be expressed in terms of the liquid water saturation. So the relation between the capillary pressure and the fluid saturation must be prescribed. In the existing literatures, the Leverette function [13] is applied extensively to relate the capillary pressure and the liquid phase saturation [14] as follows:

$$p_c = -\sigma \cos(\theta_c) \left(\frac{\varepsilon}{K_p}\right)^{1/2} J(s) \tag{7}$$

where σ and θ_c are the surface tension and contact angle, respectively. In order to remove the excessive liquid water inside the electrode, the electrode is generally made of a hydrophobic material with a contact angle greater than 90°. In this case, the Leverette function $J(s)$ takes the following form:

$$J(s) = 1.417 - 2.120s^2 + 1.263s^3 \tag{8}$$

Substituting Eqs. (4)–(8) into Eq. (3) yields the following transport equation of liquid water in term of the saturation:

$$\nabla \left[\frac{\vec{K}_{rl} \sigma \cos(\theta_c) \left(\frac{\varepsilon}{K_p}\right)^{1/2}}{\nu_l} \frac{dJ(s)}{ds} \nabla s \right] = \dot{m} \tag{9}$$

where $\dot{m}$ is the volumetric production rate of liquid water. From Eq. (9), it can be seen that the liquid water transport is driven by the capillary force and from high to low saturation region.

2.2.3. Tafel kinetics

Because the cathode kinetics is sufficiently sluggish, Bulter–Volmer kinetics [15] can be simplified to Tafel equation to determine the local transfer current along the cathode catalyst layer:

$$j_c = (1-s) i_0^{ref} a_\nu \frac{c_{O_2}}{c_{O_2}^{ref}} \exp\left(-\frac{\alpha_{c,c} F}{RT} \eta_c\right) \tag{10}$$

in which, a_ν is the specific surface area of the active sites, $c_{O_2}^{ref}$ and i_0^{ref} is the reference oxygen concentration and exchange current density on the standard condition of 1 atm and 25 °C, respectively. $\alpha_{c,c}$ is the transfer coefficient of cathodic charge in the oxygen reduction reaction, η_c is the cathode overpotential. The factor $(1-s)$ is adopted to take into account the effect of liquid water on the local transfer current density. When liquid water is present in the catalyst layer, it will cover some available reaction sites of the electrochemical reaction and prevent portion of oxygen approaching to the reaction site. The above Tafel equation implies that at the constant temperature, the local exchange current density at the cathode is a function of the oxygen concentration in the catalyst layer and the cathode overpotential. In the present work, η_c is considered as a set parameter.

2.3. Boundary conditions

At the inlet of the GDL, the oxygen molar concentration is assumed to be known:

$$c = c_0 \tag{11}$$

At the GDL–CL interface, the concentration and flux of oxygen are conserved and continuous.

$$c|_{GDL} = c|_{CL} \tag{12}$$

$$-D_{eff}^{GDL} \nabla c\big|_{GDL} = -D_{eff}^{CL} \nabla c\big|_{CL} \tag{13}$$

At the CL–PEM interface, no oxygen leaves the catalyst layer into PEM, so,

$$\nabla c = 0 \tag{14}$$

For liquid water, at the inlet of GDL, the boundary value is prescribed.

$$s = s_0 \tag{15}$$

At the GDL–CL interface, the following conditions are satisfied.

$$p_c|_{GDL} = p_c|_{CL} \tag{16}$$

$$J_w\big|_{GDL} = J_w\big|_{CL} \tag{17}$$

At the CL–PEM interface, the gradient of capillary pressure is zero, so,

$$\nabla s = 0 \tag{18}$$

The present model is solved simultaneously in the two separate and different regions, namely GDL and CL. The above transport equations along with the boundary conditions are discretized using the control volume difference method. Then, the nonlinear and coupled algebraic equations are solved by the iterative solution algorithm with under-relaxation. At each iteration level, the set of algebraic equations are solved using the standard Thomas algorithm for tridiagonal matrix. A relative convergence tolerance of 10^{-7} is used.

Table 1
Summary of parameters in the simulation.

Gas diffusion layer properties	
Porosity (ε^{GDL})	0.7 [16]
Thickness (L^{GDL})	300 μm [17]
Permeability (K_0^{GDL})	1.0×10^{-12} m^2 [18]
Tortuosity (τ^{GDL})	1.5 [6]
Catalyst layer properties	
Porosity (ε^{GDL})	0.25 [17]
Thickness (L^{GDL})	50 μm [19]
Permeability (K_0^{GDL})	$1.0 \times 10^{-1\,3}$m^2 [18]
Tortuosity (τ^{GDL})	1.5 [6]
Operation conditions	
Temperature (T)	353.15 K [20]
Pressure (p)	1.0 atm [20]
Physical properties for oxygen	
Diffusivity (D_{O_2})	0.263 cm^2 s^{-1} [14]
Physical properties of liquid water	
Kinetics viscosity (ν_l)	3.5185×10^{-7} m^2 s^{-1} [21]
Surface tensor (σ)	0.0625 N m^{-1} [21]
Reference parameters	
Transfer current ($a_v i_0^{ref}$)	5.0×10^{-4} A cm^{-3} [14]
Oxygen concentration ($c_{O_2}^{ref}$)	4.62×10^{-6} mol cm^{-3} [14]
Cathode transfer coefficient ($a_{c,c}$)	2 [14]

3. Results and discussions

The parameters and physical properties in the simulation are listed in Table 1. In which, the thickness of the catalyst layer is a litter thicker than one commonly used in some literatures to give prominence to the profiles in the thin layer. The effect of the CL thickness on the flooding level will be further assessed.

3.1. Profiles of oxygen concentration and liquid saturation

Fig. 2 shows the comparison of oxygen concentration distributions when no and some amount of liquid water present in the cathode with the current density is 0.68 Acm^{-2}. Meanwhile, the responding liquid water saturation distribution is also plotted in the figure. From Fig. 2, it can be clearly seen that the reduction of oxygen concentration along the electrode in the case of flooding is relatively smaller than that of no liquid water existing. It is the reason that liquid water occupies portion of the pore space of oxygen transport path, which increases the resistance to the oxygen transport and hinders some amount of oxygen approaching to the active sites of the catalyst layer. Consequently, the amount of oxygen participating in the oxygen reduction reaction (ORR) is reduced.

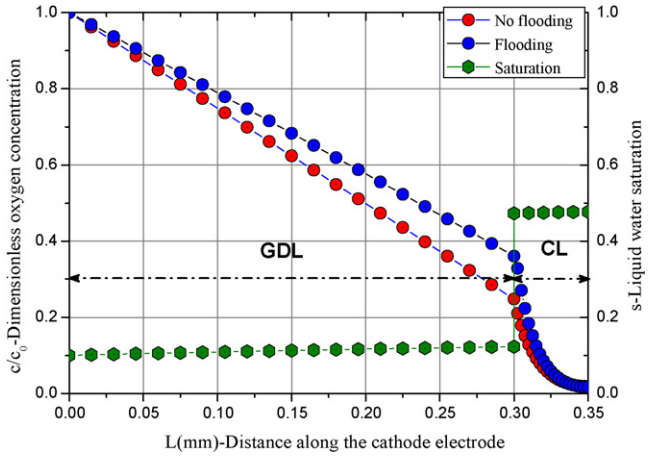

Fig. 2. Comparison of the oxygen distributions for no flooding and flooding cases.

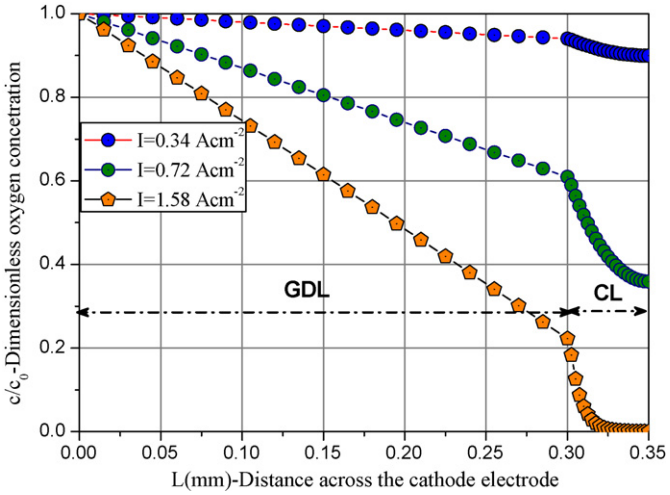

Fig. 3. Profiles of the oxygen molar concentration along the cathode electrode.

Additionally, the saturation predicted by the present model shows a reasonable agreement to the experimental results by the neutron radiography technique [22], that is, liquid water in the CL is much more than one in the GDL.

Fig. 3 shows the oxygen concentration distributions inside the cathode for different current densities. In order not to take into consideration the effect of the inlet oxygen concentration on the distribution, in the figure, the oxygen molar concentrations are reduced by the value of c_0. From Fig. 3, it can be seen that the oxygen concentration profile in the GDL is a straight line because of no consumption and production of oxygen. As a result, the mass flux of oxygen keeps constant everywhere in this region. However, inside the CL, the profile is nonlinear in that oxygen is consumed in the ORR, and the change in the mass flux gives rise to a nonlinear concentration profile.

Note also when the exchange current density also increases, and more amount of oxygen are consumed by the electrochemical reaction in the catalyst layer. When the overpotential approaches some value, oxygen fed at the inlet of the gas channel will deplete completely somewhere in the CL, seen Fig. 4. In this case, the oxygen mass transport is limited and the corresponding limiting current density is maximal.

Fig. 5 shows the liquid saturation profiles for different current densities. Firstly, it is easy to observe that the saturation is dis-

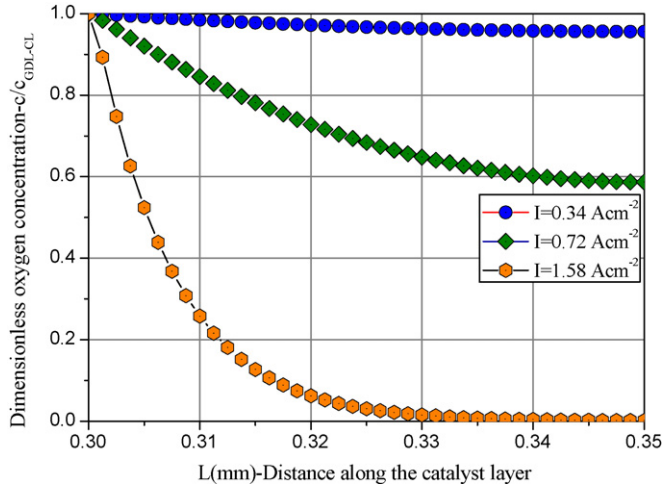

Fig. 4. Profiles of the oxygen concentration in the CL.

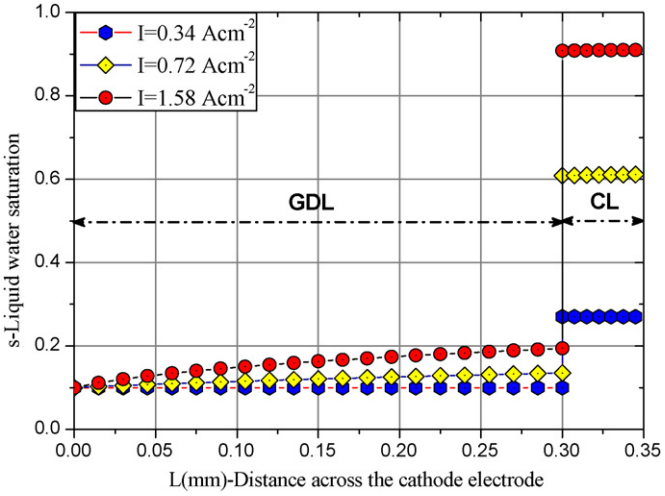

Fig. 5. Profiles of the liquid water saturation along the cathode electrode.

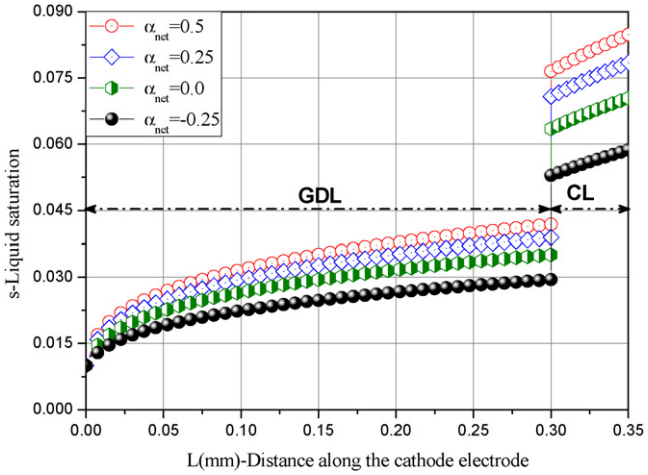

Fig. 6. Profiles of the liquid water saturation along the cathode electrode.

continuous at the GDL–CL interface, which is resulted from the interfacial condition of the capillary pressure continuity. According to the knowledge about the thermodynamic equilibrium, the mechanical equilibrium should be satisfied at the GDL–CL interface. Therefore, the pressures of both the gas and liquid phases are continuous across the interface, thus, the capillary pressure is continuous. However, the GDL and CL are significantly different in the capillary properties, such as, the porous size, permeability and wetting characteristics. In order to satisfy the capillary pressure continuity, from Eq. (7), the liquid saturation must be different on both sides of the GDL–CL interface, thereby a huge jump is captured at the interface, as shown in Fig. 5.

In addition, from Fig. 5, it is seen that the saturation increases with the increase of the current density, and the increasing degree of the saturation in the CL is much larger than one in the GDL. It implies that the flooding situation within the CL is more severe than one in the GDL. One reason is that liquid water firstly generates in the CL by the ORR and reaches prior to the cathode catalyst layer from the anode electrode. As a result, liquid water firstly accumulates in the CL. Generally, water is transported out of the catalyst layer by three means, evaporation and gas-phase diffusion, capillary flow and back diffusion across the membrane from the cathode to the anode. In the present work, phase transition is not considered, so the liquid water accumulating in the CL is transported only by both the capillary force and back diffusion. Other reasons are the saturation gradient is needed for the capillary flow and the CL permeability is relatively smaller than the GDL permeability, consequently, the saturation level in the CL is much higher than that in the GDL. Therefore, in order to prevent flooding, the liquid water staying inside the CL must be firstly transported out.

3.2. Influence parameters on the saturation profiles

In this section, the influence parameters on the saturation distribution are investigated.

3.2.1. The net transport coefficient

The water transport across the membrane from the anode to the cathode is governed by three mechanisms [23]: water molecules migrated by the electro-osmotic drag due to the electrical potential gradient, back diffusion due to the concentration gradient and convective flux due to the pressure gradient. The net water transport coefficient, α, can be used to represent the net amount of water transport from the anode to the cathode. It can be further defined as the number of water molecules transported across the membrane per proton. So that the liquid water mass flux is given by:

$$J_{\mathrm{m}} = (2\alpha + 1)\frac{I}{2F} \tag{19}$$

here J_{m} is the mass flux of liquid water per unit area of the electrode, I is the mean current density with the unit of A cm^{-2}.

In Fig. 6, the liquid saturation profiles are plotted for different net transport coefficients. When α equals to zero, it means that liquid water in the cathode electrode is produced only by the oxygen reduction reaction, as the above results shown. If α is larger than zero, liquid water is formed as a combined result of the ORR and the transport across the membrane from the anode to the cathode. And the negative α leads portion of liquid water generated by the electrochemical reaction to transport from the cathode to the anode due to the concentration gradient between both electrodes. As shown in Fig. 6, when the net transport coefficient enhances, more amount of liquid water will transport across the membrane from the anode to the cathode and accumulate within the CL. So that, under the condition of the same overpotential, the saturation level within the GDL and CL enhance, which is much easier to flood.

3.2.2. The boundary value of liquid saturation

The boundary value of saturation at the inlet of the GDL depends on the size, shape and number of the liquid droplets covering the GDL surface, and is thus a function of such parameters as the channel gas velocity and GDL surface permeability [24]. In some literatures, zero value is used. Fig. 7 shows the liquid saturation profiles for the different boundary values. It can be evidently seen that the effect of the boundary value of the liquid saturation at the GDL–gas channel interface on the liquid water accumulation level inside the cathode is very extreme. Very small change in the boundary value will result in the significant difference of the saturation value on two sides of the GDL–CL interface. For example, if the boundary value of liquid saturation changes from 0.1 to 0.2, the saturation jump will reach up to almost 50%. In addition, if the boundary value at the GDL–gas channel approaches to zero, the saturation profile is nonlinear approximately as the parabola shape within the GDL. However, upon enhancing this boundary value, the saturation profiles present different curve shapes, and become more linear, meanwhile, the saturation levels in both GDL and CL increase. It implies that the water saturation at the cathode GDL–CL interface increases with the increase of the water saturation at the GDL–gas channel interface. Therefore, if it is expected more reactant gases to transport into the catalyst layer, the liquid saturation at the GDL–gas channel interface should be kept as low as possible.

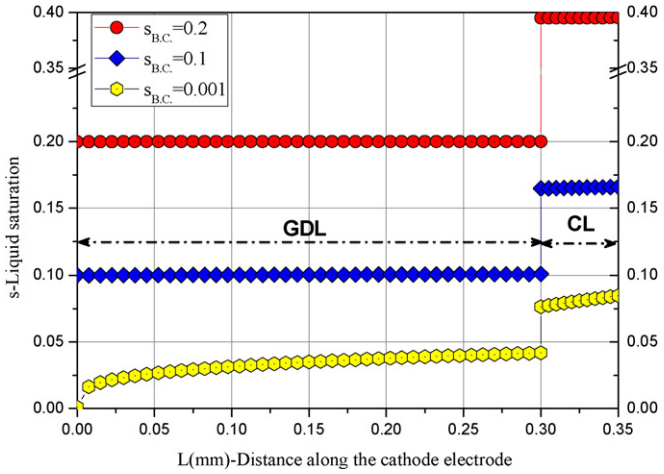

Fig. 7. Variation of the liquid saturation with the boundary value.

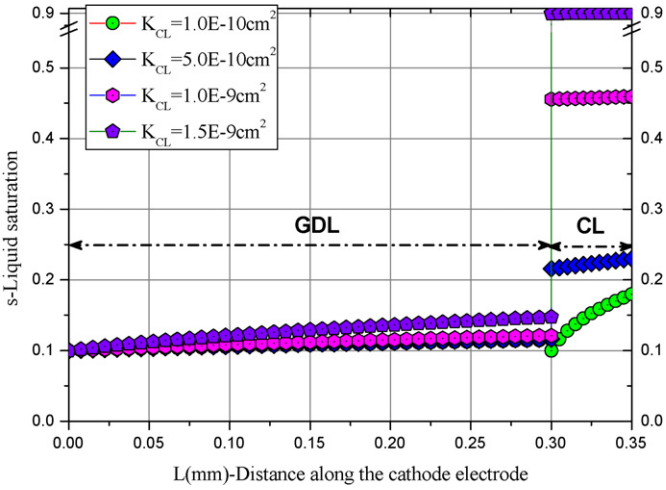

Fig. 8. Variation of the liquid water saturation with permeability of CL.

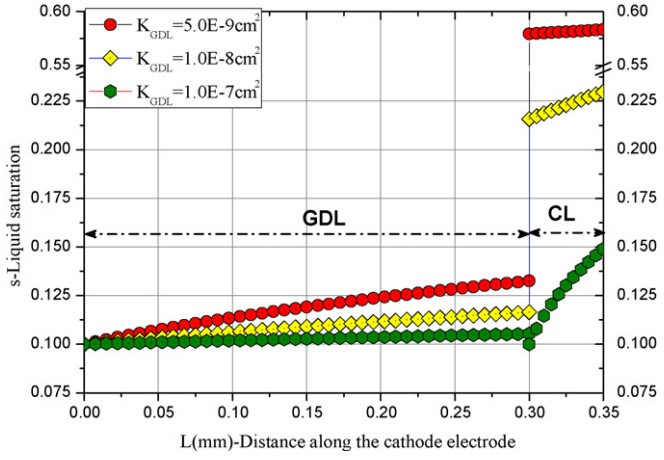

Fig. 9. Variation of the liquid water saturation with permeability of GDL.

3.2.3. *The absolute permeability*

The absolute permeability of the porous media is a measurement of the material ability to transmit a fluid on the condition of the dry state. The fluid penetrates more difficultly across the porous medium with the smaller permeability. Figs. 8 and 9 show the change of the liquid water saturation with the different absolute permeability of the GDL and CL, respectively. They indicate that the saturation level within the cathode GDL increases with the reduction of the GDL permeability and the saturation jump on the side of CL enhances with the increase of the CL permeability, which suggests the predicated saturation levels largely depend on the permeability of the porous medium. In the case of the same mass flux, the amount of liquid water remaining in the porous media is enhanced due to the smaller permeability, so the slop of the linear liquid saturation profile becomes lager, which will result in a larger jump at the GDL–CL interface.

4. Conclusions

A two-phase, one-dimensional model has been developed for the cathode of the proton exchange membrane fuel cells, and the phenomena of mass-transport limitation and flooding occurring are investigated with the capillary pressure condition.

Because of the distinct capillary properties of the GDL and CL, in order to satisfy the continuity interfacial condition of the capillary pressure and the conservation of the mass flux at the GDL–CL interface, a huge jump of saturation is captured at the interface. So that most of liquid water accumulate within the cathode electrode and lead to the flooding, if the excessive liquid water is not efficiently removed. Furthermore, it is further confirmed that the flooding situation in the CL is much more serious than that in the GDL, since liquid water produced in the electrochemical reaction originates in the catalyst layer.

If once the flooding takes place within the catalyst layer, liquid water will fill the catalyst layer pores, which may further cover the active sites in the catalyst layer and block oxygen transporting to the active sites and render them electrochemically inactive, so the oxygen transport flux across the CL is limited, and the mass-transport limitation emerges.

In order to understand how to remove effectively the liquid water accumulated in the cathode, the effects of some important parameters, such as the boundary value of the saturation, the net transport coefficient and the permeability, on the saturation level are investigated. The chosen values of these parameters must make the removal rate of liquid water greater than its production rate, which can prevent simultaneously the flooding and mass-transport limitation phenomena occurring, so that the reactant gases would approach the active sites with smaller transport resistance.

Acknowledgments

The authors would like to thank NEDO (New Energy and Industrial Technology Development Organization) of Japan for the financial support for this research.

References

[1] W.S. He, J.S. Yi, T.V. Nguyen, AIChE J. 46 (10) (2000) 2053–2064.
[2] D. Natarajan, T.V. Nguyen, J. Electrochem. Soc. 148 (12) (2001) A1324–1335.
[3] M. Najjari, F. Khemili, S.B. Nasrallah, Renewable Energy 33 (2008) 1824–1831.
[4] M. Eikerling, J. Electrochem. Soc. 153 (3) (2006) E58–70.
[5] A.Z. Weber, J. Newman, Chem. Rev. 104 (10) (2004) 4679–4726.
[6] D.M. Bernardi, M. Verbrugge, J. Electrochem. Soc. 139 (9) (1992) 2477–2491.
[7] L.X. You, H.T. Liu, Int. J. Hydrogen Energy 26 (2001) 991–999.
[8] N.P. Siegel, M.W. Ellis, D.J. Nelson, M.R. Spakovesky, J. Power Sources 115 (2003) 81–89.
[9] M.K. Baboli, M.J. Kermani, Electrochim. Acta 53 (2008) 7644–7654.
[10] R.E. Meredith, C.W. Tobias, Advances in Electrochemical Science and Engineering, 2nd ed., Interscience, New York, 1962.
[11] J. Bear, Dynamics of Fluids in Porous Media, Elsevier, New York, 1972.
[12] C.Y. Wang, P. Cheng, Adv. Heat Mass Transf. 30 (1997) 93–196.
[13] M.C. Leverett, Trans. AIME 142 (1941) 152–169.
[14] K.T. Jeng, S.F. Lee, G.F. Tsai, C.H. Wang, J. Power Sources 138 (2004) 41–50.
[15] M. Matthew, Fuel Cell Engines, John Wiley & Sons, Inc., Hoboken, NJ, 2008.
[16] D.H. Ahmed, H.J. Sung, J. Bae, Int. J. Hydrogen Energy 33 (2008) 3767–3785.
[17] L.X. You, H.T. Liu, J. Power Sources 155 (2006) 219–230.

[18] H. Meng, J. Power Sources 168 (2007) 218–228.
[19] A.A. Kulikovskya, J. Electrochem. Soc. 150 (2003) A1432–A1439.
[20] S. Litster, J.G. Pharoah, G. McLean, N. Djilali, J. Power Sources 156 (2006) 334–344.
[21] F.P. Incropera, D.P. DeWitt, Fundamentals of Heat and Mass Transfer, John Wiley and Sons, New York, 1996.
[22] M.A. Hickner, N.P. Siegel, K.S. Chen, D.S. Hussey, D.L. Jacobson, M. Arif, J. Electrochem. Soc. 155 (2008) B427–B434.
[23] L. You, H. Liu, Int. J. Heat Mass Transf. 45 (2006) 2277–2287.
[24] U. Pasaogullari, C.Y. Wang, K.S. Chen, J. Electrochem. Soc. 151 (8) (2005) A1574–A1582.